Journal of Materials Chemistry B

Synthesis and Photophysical Properties of a New Push–Pull Pyrene Dye with Green-to-Far-red Emission and its Application to Human Cellular and Skin Tissue Imaging

Journal:	*Journal of Materials Chemistry B*
Manuscript ID	TB-ART-12-2021-002728.R1
Article Type:	Paper
Date Submitted by the Author:	27-Jan-2022

Complete List of Authors:

Inoue, Kazuki; Kochi University, Research and Education Faculty, Multidisciplinary Science Cluster, Interdisciplinary Science Unit
Kawakami, Ryosuke; Ehime University Graduate School of Medicine, Department of Molecular Medicine for Pathogenesism
Murakami, Masamoto; Ehime University Graduate School of Medicine, Department of Dermatology
Nakayama, Taku; Kochi University, Center for Photodynamic Medicine Kochi Medical School
Yamamoto, Shinkuro; Kochi University, Center for Photodynamic Medicine Kochi Medical School
Inoue, Keiji; Kochi University, Center for Photodynamic Medicine Kochi Medical School
Tsuda, Teruko; Ehime University Graduate School of Medicine, Department of Dermatology
Sayama, Koji; Ehime University Graduate School of Medicine, Department of Dermatology
Imamura, Takeshi; Ehime University Graduate School of Medicine, Department of Molecular Medicine for Pathogenesism
Kaneno, Daisuke; Kochi University, Department of Applied Science, Graduate School of Integrated Arts and Sciences
Hadano, Shingo; Kochi University, Research and Education Faculty, Multidisciplinary Science Cluster, Interdisciplinary Science Unit
Watanabe, Shigeru; Kochi University, Research and Education Faculty, Multidisciplinary Science Cluster, Interdisciplinary Science Unit
Niko, Yosuke; Kochi University, Research and Education Faculty, Multidisciplinary Science Cluster, Interdisciplinary Science Unit

ARTICLE

Synthesis and Photophysical Properties of a New Push–Pull Pyrene Dye with Green-to-Far-red Emission and its Application to Human Cellular and Skin Tissue Imaging

Received 00th January 20xx,
Accepted 00th January 20xx

DOI: 10.1039/x0xx00000x

Kazuki Inoue,[†a] Ryosuke Kawakami,[†b] Masamoto Murakami,[c] Taku Nakayama,[d] Shinkuro Yamamoto,[d] Keiji Inoue,[d] Teruko Tsuda,[c] Koji Sayama,[c] Takeshi Imamura,[b] Daisuke Kaneno,[e] Shingo Hadano,[a] Shigeru Watanabe[a] and Yosuke Niko*[a]

Herein, we discuss a new pyrene-based push–pull dye (**PC**) and our investigation of its photophysical properties and applicability to biological applications. The newly synthesized dye exhibits highly polarity-sensitive fluorescence over a significantly wide range (*i.e.*, green to far-red region), accompanied by high fluorescent quantum yields (Φ_{FL} > 0.70 in most organic solvents) and superior photostability to that of the commonly used Nile Red (**NR**) dye, which also fluoresces in the green to red region. When human prostate cancer cells stained with **PC** were imaged using a confocal laser scanning fluorescence microscope, **PC** was found to selectively stain the lipid droplets. Under the cell conditions where the formation of droplets was inhibited, **PC** could be distributed to both the remaining droplets and the intercellular membranes, which could be distinguished based on the fluorescence solvatochromic function of **PC**. Furthermore, **PC** efficiently stained normal human skin tissue blocks treated with a transparency-enhancing agent and enabled the clear visualization of individual cells in each tissue architecture by means of two-photon fluorescence microscopy (2PM). Interestingly, **PC** provides bright 2PM images under tissue-penetrative 960-nm excitation, realizing much clearer and deeper tissue imaging than conventional pyrene dyes and **NR**. These results suggest that **PC** could replace several commonly used dyes in various biological applications, particularly the rapid and accurate diagnosis of tissue diseases, typified by biopsy.

Introduction

Push–pull dyes are molecules bearing electron-donor and -acceptor groups connected via a π-conjugated system, giving them simple frameworks that are suitable for developing fluorescent materials.[1–11] Their push–pull design allows for the energy gap between the highest occupied molecular orbital and lowest unoccupied molecular orbital to be varied, thus enabling the control of their absorption and fluorescence wavelengths. Furthermore, push–pull dyes often take on an intramolecular charge transfer (ICT) state upon photoexcitation, resulting in a large Stokes shift and polarity-sensitive fluorescence photofunction. Thus, the push–pull motif has been applied to develop new fluorescent dyes, particularly small molecular fluorescent probes for detecting biomolecular interactions,[12] mapping polarities in cell organelles,[13] or monitoring the lipid order (i.e., the degree of lipid organization/lipid packing) in biomembranes;[12,14,15] such applications require probes with several specific chemical, physical, and photophysical properties.

Push–pull dyes composed of pyrene as the core π-conjugation system have attracted considerable attention for their use in spectroscopic and microscopic applications in biological studies owing to their excellent brightness, photostability, and highly polarity-sensitive solvatochromic fluorescence (Figure 1).[11,16–19] Among them, pyrene derivatives substituted with a piperidyl group as an electron donor and either a formyl or ketone group as an electron acceptor, **PA** and **PK**, respectively, were recently found to rapidly distribute cell plasma and intracellular membranes in living cells and denote the lipid order of lipid membranes by changing their fluorescence color.[18,19] This feature is useful for studying various cellular phenomena related to membrane processes.[14,15] **PK** is currently commercially available, and more recently, it was found to efficiently stain the cell membranes in paraffin-embedded or frozen human skin tissue blocks, enabling the visualization of

[a] *Research and Education Faculty, Multidisciplinary Science Cluster, Interdisciplinary Science Unit, Kochi University, 2-5-1 Akebono-cho, Kochi-shi, Kochi 780-8520, Japan.*
[b] *Department of Molecular Medicine for Pathogenesism, Graduate School of Medicine, Ehime University, Shitsukawa, Toon, Ehime 791-0295, Japan.*
[c] *Department of Dermatology, Graduate School of Medicine, Ehime University, Shitsukawa, Toon, Ehime 791-0295, Japan*
[d] *Center for Photodynamic Medicine, Kochi Medical School, Kochi University, Kohasu, Oko-cho, Nankoku, Kochi 783-8505, Japan.*
[e] *Department of Applied Science, Graduate School of Integrated Arts and Sciences, Kochi University, 200 Otsu, Monobe, Nankoku City, Kochi 783-8502, Japan.*
*Corresponding author. E-mail: y.niko@kochi-u.ac.jp
†These authors contributed equally to this work.

Electronic Supplementary Information (ESI) available: Synthetic procedure of **PC** and its ^{1}H and ^{13}C NMR spectra; absorption spectra of **PC** and **PK** in organic solvents and LUVs; evaluation of the dependence of dye's Stokes shift on polarity index using Lippert-Mataga' and Bakhshiev's equations; time-resolved fluorescence decay of PC in LUVs of different lipid compositions; Cytotoxicity of **PC** and **PK** using human keratinocyte K16.
. See DOI: 10.1039/x0xx00000x

the individual cell morphologies in a three-dimensional manner through two-photon fluorescence microscopy (2PM);[20] this is useful for the rapid and accurate diagnosis of human skin diseases.[21] Notably, most existing pyrene-based push–pull dyes exhibit fluorescence in the blue-to-yellow region (Figure 1). On the other hand, dyes emitting in longer-wavelength regions (e.g., orange-to-far-red or even near-infrared regions) are believed to be potentially advantageous for bio-imaging applications, such as deep-tissue imaging, requiring excitation/fluorescence lights with such tissue-penetrative wavelengths to minimize light-scattering and autofluorescence.[22] Motivated by these considerations, we developed a minimally π-extended analog of **PK** (**PC**) as a new pyrene dye and compared its photophysical properties and applicability to biological applications to those of conventional dyes like **PK**[19] and Nile Red (**NR**).[2]

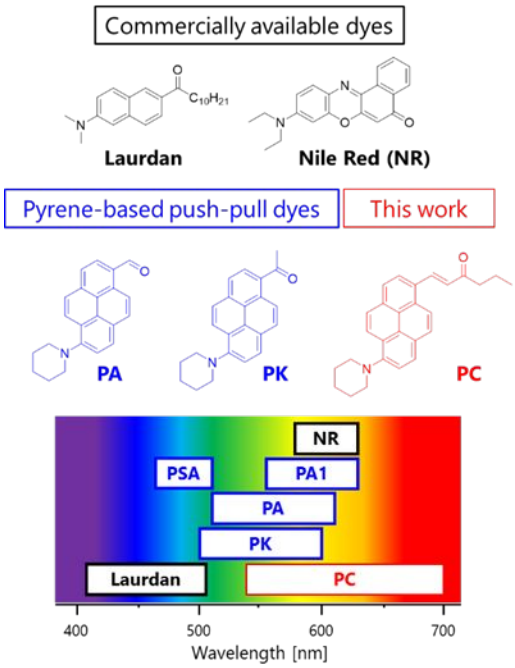

Figure 1. Molecular structures of (top) commercially available and (middle) pyrene-based push–pull dyes and (bottom) their emission ranges. Laurdan, PSA, and PA1 are described in references 23, 16, and 17, respectively.

Result and Discussion

Molecular design and synthesis of PC

Among the options for designing a pyrene-based push–pull dye with longer absorption and fluorescence wavelengths than those of **PK**, we decided to replace the ketone acceptor moiety of **PK** with a stronger, π-extend vinyl ketone group.[24] Because the resulting new dye, **PC**, has a structure similar to that of **PK**, it is expected to exhibit a high affinity to lipid membranes (*i.e.*, an applicability to cellular and tissue imaging) like **PK**.[19] In addition, such direct π-extension of a pyrene dye using a vinyl group is expected to increase the two-photon absorption cross-section of the dye and induce red-shifts in both its absorption and fluorescence wavelengths.[25,26]

The synthetic route toward **PC** is outlined in Scheme S1. Briefly, **PC** was easily synthesized from previously reported **PA** via an aldol condensation.[18] The structure of **PC** was characterized by ^{1}H and ^{13}C NMR spectroscopy and high-resolution mass spectroscopy (see Supporting Information). Alternatively, **PC** derivatives were prepared from 1,6-dibromopyrene in two steps: Buchwald–Hartwig amination[27] and a subsequent Heck reaction[28] (see Supporting Information). Consequently, this route can provide **PC** derivatives applicable to specific biological applications.

Absorption and fluorescence properties of PC in organic solvents

The absorption and fluorescence spectra of **PC** were recorded in several solvents of different polarities and compared with those of **PK** (Figures 2a, 2b, and S1). The absorption maximum wavelengths ($\lambda_{max,\ abs}$) of **PC** in all the tested solvents were located around 420 nm, demonstrating that it is not very sensitive to solvent polarity (Table 1). This spectral behavior of **PC** is similar to that of **PK** and indicates that both molecules have small dipole moments in the ground state. The $\lambda_{max,\ abs}$ values of **PC** are red-shifted by approximately 20 nm compared to those of **PK**; additionally, the extinction coefficients of **PC** are slightly larger than those of **PK**, likely because the former has a longer electronic conjugation owing to its vinyl group.

The spectral differences between **PC** and **PK** were further emphasized in their fluorescence spectra; **PC** exhibits fluorescence over a region of green to far-red, which is significantly red-shifted compared to that of **PK**. The maximum fluorescence wavelength ($\lambda_{max,\ FL}$) of **PC** strongly depended on the solvent polarity (i.e., solvatochromic fluorescence). For instance, its $\lambda_{max,\ FL}$ values in toluene and acetonitrile differed by about 95 nm, which is a much larger difference than those noted for **PK** (45 nm) and **NR** (48 nm)[17] in the same solvents; **NR** fluoresces in the green to red region. To quantitatively describe such solvatochromic fluorescence, the correlation between the fluorescence band positions of **PC** and **PK** and their polarity index $E_T(30)$[29] values was studied (Figure 2c). A good linear correlation was obtained for both **PC** and **PK**, which is common for solvatochromic dyes employing ICT mechanisms. The slope obtained for **PC** (187 cm^{-1}) was steeper than that determined for **PK** (125 cm^{-1}), indicating that **PC** exhibits a stronger fluorescence solvatochromic response than **PK**. To further understand this phenomenon, the changes in the dipole moments ($\delta\mu$) of the ground (μ_g) and excited states (μ_g) of **PC** and **PK** were studied using the correlation between their Stokes shifts ($\nu_a - \nu_f$) and Reichardt's solvent parameters (E_T^N),[29] and Ravi's equation.[30] As shown in Figure 2d, both **PC** and **PK** showed good linear correlations, and their slopes were 5,337 cm^{-1} and 3,911 cm^{-1}, respectively. From these data, the $\delta\mu$ values of **PC** and **PK** were estimated as 3.94 D and 3.18 D (1 D = 3.33564×10^{-30} cm = 10^{-18} esu cm), respectively; other equations used to estimate $\delta\mu$ (e.g., the Lippert–Mataga[31] and Bakhshiev[32] equations) showed the same trend, with **PC** having larger $\delta\mu$ values than **PK** (Figure S2 and Table S1). A similar trend was observed for the theoretical $\delta\mu$ values obtained using density

functional theory (DFT)/time-dependent DFT (TDDFT) calculations (Figure S3). These results suggest that **PC** has more pronounced ICT characteristics than **PK**, simply due to the vinyl ketone of the former being a stronger electron acceptor group than the ketone of the latter; therefore, **PC** exhibits a larger Stokes shift and stronger fluorescence solvatochromism than **PK**.

Moreover, **PC** exhibited a sufficiently high fluorescence quantum yield (Φ_{FL}: ~0.80) in most solvents, as did **PK** (Table 1). However, the Φ_{FL} of **PC** rapidly decreased in highly polar and protic solvents, including phosphate buffer (PB), which is a common behavior of push–pull dyes with high $\delta\mu$ values.[8–10] This is probably due to the formation of a charge-separated ICT state in the excited state[33] with subsequent thermal deactivation, or dye aggregation in water.[12] It should be noted that such a decrease in Φ_{FL} observed in highly polar solvents is often advantageous for bio-imaging, specifically wash-free fluorescence imaging.[15]

To estimate the photostability of **PC**, a photodegradation curve under continuous light illumination was studied. Here, we selected toluene as a solvent because push–pull dyes tend to exhibit efficient intersystem crossing to their excited triplet states in low-polarity solvents, which results in the generation of singlet oxygen via energy transfer and subsequent photodegradation of the dyes. As shown in Figure 3a, **PC** and **PK** maintained 95% and 90%, respectively, of their initial fluorescence intensities after 3 h of irradiation, indicating that **PC** has photostability comparable to or better than that of **PK**. Similarly, the photostability of **PC** was compared with that of **NR**. Although **NR** has been widely used for several imaging techniques,[34–36] including stimulated emission depletion microscopy (STED),[35] which requires sufficiently photostable fluorescent probes, its photostability and associated photo-toxicity are significant drawbacks to its application.[37,38] Interestingly, while **NR** only maintained 76% of its initial fluorescence intensity after 3 h of irradiation, **PC** maintained 93% of its initial fluorescence intensity, indicating that **PC** has superior photostability to **NR** (Figure 3b). Considering that **PC** exhibits better sensitivity to environmental polarity than **NR**, and because its fluorescence is more red-shifted, it could be preferable to **NR** in cellular imaging where the photostability of the probe is crucial, e.g. long-term imaging and super-resolution imaging.

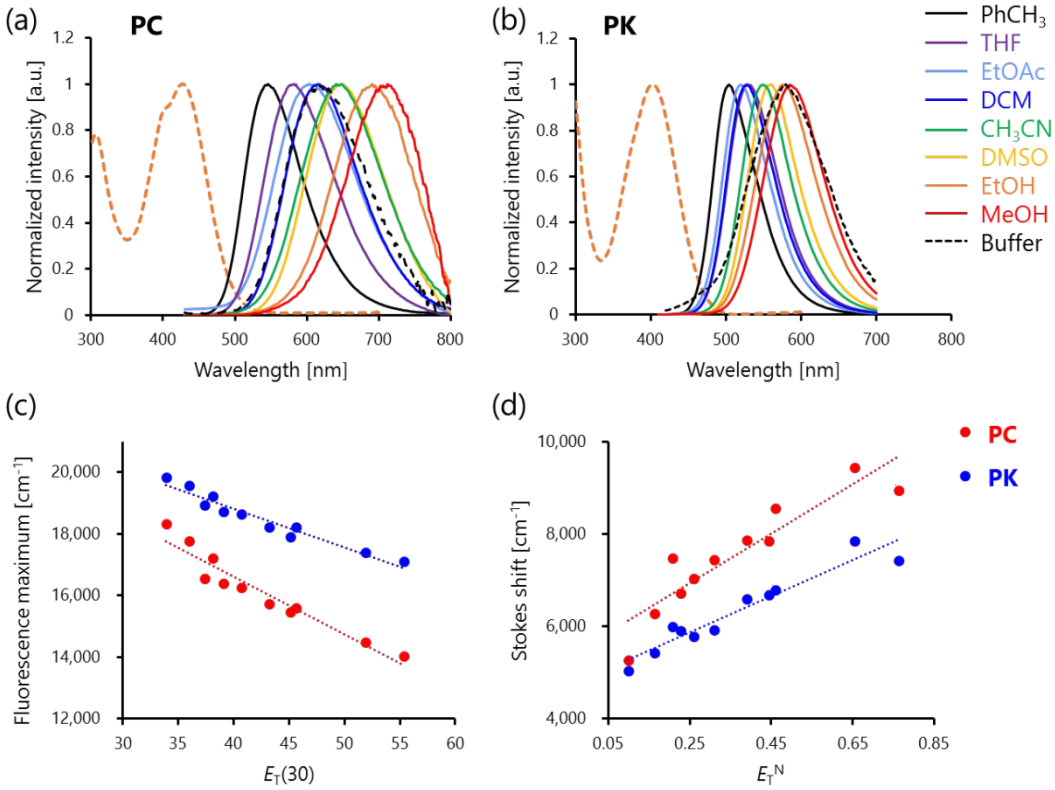

Figure 2. (a, b) Absorption (dotted line, ethanol solution) and fluorescence (solid line) of (a) the newly (**PC**) and (b) previously (**PK**) developed pyrene-based push–pull dyes in organic solvents of different polarities. (c) Position of the emission maxima of **PC** (red) and **PK** (blue) versus their polarity index ($E_T(30)$) values in aprotic solvents. The r^2 (goodness of fit) values of **PC** and **PK** are 0.93 and 0.94, respectively. (d) The variation in the Stokes shifts of **PC** (red) and **PK** (blue) with the microscopic solvent function (E_T^N); their r^2 values are 0.84 and 0.91, respectively.

Table 1. Comparison of the spectroscopic parameters of **PC** and **PK** in organic solvents and large unilamellar vesicles (LUVs).[a]

Solvent/LUV	$E_T(30)$ [b]	E_T^N [c]	PC $\lambda_{max, abs}$ [nm]	PC $\lambda_{max, FL}$ [nm]	PC Φ_{FL}	PK $\lambda_{max, abs}$ [nm]	PK $\lambda_{max, FL}$ [nm]	PK Φ_{FL}
Toluene	33.9	0.099	424	546	0.82	402	504	0.80
Dioxane	36	0.164	416	563	0.81	400	511	0.88
THF	37.4	0.207	416	604	0.74	401	528	0.79
Ethyl acetate	38.1	0.228	418	581	0.77	398	520	0.75
Chloroform	39.1	0.259	427	610	0.83	408	534	0.86
Dichloromethane	40.7	0.309	422	615	0.86	407	536	0.88
DMF	43.2	0.39	424	636	0.77	403	549	0.80
DMSO	45.1	0.444	429	647	0.79	407	559	0.82
Acetonitrile	45.6	0.46	414	641	0.65	400	549	0.76
Ethanol	51.9	0.762	427 [d]	691	0.20	403 [d]	575	0.77
Methanol	55.4	0.654	426	712	0.07	401	585	0.73
PB (20 mM, pH = 7.2)	-	-	426	618	0.05	403	580	0.08
DOPC	-	-	429	603	0.37	405	569	0.45
SM/Chol	-	-	433	577	0.72	413	513	0.59

a: Definitions. $\lambda_{max, abs}$ = maximum absorption wavelength, $\lambda_{max, FL}$ = maximum fluorescence wavelength, Φ_{FL} = fluorescence quantum yield, THF = tetrahydrofuran, DMF = *N*,*N*-dimethylformamide, DMSO = dimethyl sulfoxide, PB = phosphate buffer, DOPC = 1,2-dioleoyl-sn-glycero-3-phosphocholine, SM/Chol = sphingomyelin/cholesterol. b and c: These data were obtained from ref 27. d: The extinction coefficients of **PC** and **PK** in ethanol are 27,500 M^{-1} cm^{-1} and 17,400 M^{-1} cm^{-1}, respectively.

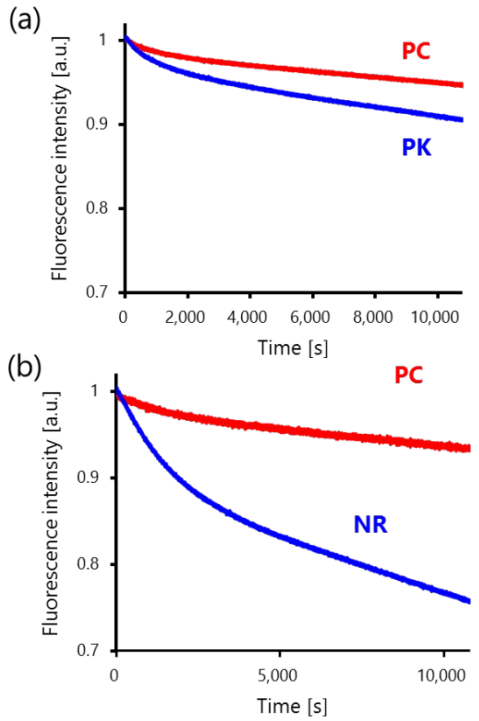

Figure 3. Photodegradation of **PC**, **PK** and Nile Red (**NR**) in toluene. Excitation wavelengths used to evaluate (a) **PC** vs **PK** and (b) **PC** vs **NR** were 373 nm and 460 nm, respectively, and were determined from the cross points of the absorption spectra of each dye in a 5 μM solution.

Fluorescence behavior of PC in large unilamellar vesicles with different lipids

Prior to the use of **PC** for biological applications, it would be valuable to study whether the dye could bind to lipid structures and to determine its sensitivity to lipid composition. Herein, we employed large unilamellar vesicles (LUVs) composed of sphingomyelin/cholesterol (SM/Chol) and 1,2-dioleoyl-sn-glycero-3-phosphocholine (DOPC), which are often used as models of cell plasma membranes and intracellular membranes, respectively.[14,15] As expected, **PC** rapidly bound to both LUVs, similar to **PK**, and exhibited different fluorescence spectra in response to lipid composition (Figures 4a and 4b and Table 1). When **PC** was added to LUVs comprising SM/Chol, which are known to have highly packed structures, the dye exhibited green to yellow emission around 580 nm with a high Φ_{FL} value (0.72). On the other hand, when **PC** was added to LUVs consisting of DOPC, which have loosely packed structures, it exhibited significantly broad and relatively weak fluorescence in a red-shifted area ($\lambda_{max, FL}$ = 603 nm, Φ_{FL} = 0.37). Such differences in the fluorescence behavior of **PC** in LUVs comprising SM/Chol or DOPC reflect the differences in the LUV microenvironments. LUVs composed of SM/Chol are known to have low water contents and polarities because of their highly packed structures, allowing **PC** to fluoresce at relatively short wavelengths, as if in a low-polarity solvent. In contrast, DOPC LUVs have high water contents and polarities due to their loosely packed structures, enabling **PC** to exhibit fluorescence at long wavelengths with low Φ_{FL} values, as if in a polar and protic solvent. Such a spectral change observed for **PC** in these different LUVs is consistent with those observed for other ICT-based fluorescence solvatochromic dyes, including Laurdan,[18] **NR**,[34] and **PK**.[19] On the other hand, the spectral shift observed for **PC** in SM/Chol and DOPC LUVs was not as drastic as that demonstrated by **PK**, despite the fact that the fluorescence of **PC** is more sensitive to the polarities of organic solvents than that of **PK**. This difference between **PC** and **PK** when tested in the same organic solvents and LUVs is likely observed because **PC** has a slightly more hydrophobic structure than **PK**; therefore, **PC** penetrates deeper into the lipid bilayer than **PK** (Figure 4c), to a point where it cannot sense water molecules located at the lipid–water interface. Unfortunately, this lack of

control over the location of **PC** within lipid bilayers is an undesirable property of membrane probes used to monitor the lipid order of biomembranes in live cells by means of ratio-metric analysis.[14,15] However, this problem could be solved by modifying **PC** with an "anchor molecule" consisting of a long alkyl chain and sulfonate anion, a technique developed by Klymchenko and co-workers.[36] This modification is known to enable the control of the position of fluorescence probes in lipid bilayers; thus, such an anchor may improve the sensitivity of the **PC** fluorescence wavelength to lipid composition. On the other hand, from the analysis of time-resolved fluorescence decay of **PC**, it was revealed that the mean lifetimes of **PC** in SM/Chol and DOPC LUVs differed more than those of **PK** in the same LUVs (Figure S4). This could be explained by the Φ_{FL} value of **PC** being more sensitive to environmental polarity than that of **PK** due to its stronger ICT character, as mentioned above. Specifically, the Φ_{FL} value of **PC** tends to be low in highly polar DOPC LUVs; consequently, its fluorescence lifetime in such an environment is low. Thus, **PC** still has potential applicability as a fluorescent probe for monitoring the lipid order of lipid compartments by means of fluorescence lifetime imaging microscopy (FLIM).[14,15]

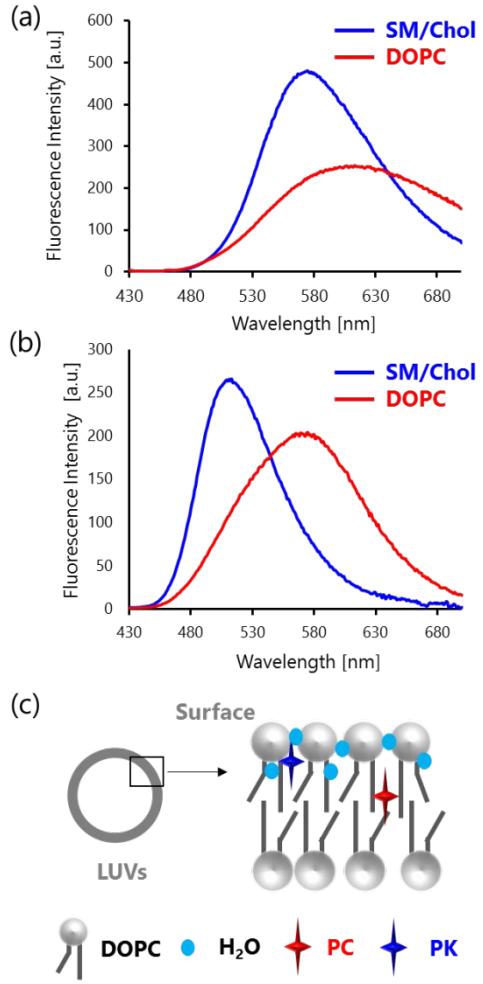

Figure 4. Fluorescence spectra of (a) **PC** and (b) **PK** in LUVs of different compositions. Dye concentration: 2 μM; lipid concentration: 200 μM (PB 20 mM, pH 7.2); excitation wavelength: 420 nm and 405 nm for **PC** and **PK**, respectively. (c) Schematic illustration of the positions of **PC** and **PK** in the LUVs.

Fluorescence microscopy applications of PC

To exploit the applicability of **PC** to biological applications, we first conducted fluorescence imaging of a human prostate cancer cell line (PC3) using confocal laser scanning fluorescence microscopy (CLSM). **PC** (0.5 μM) was incubated with live cells for 30 min and fluorescence images were acquired using two channels (green channel: 490–590 nm, red channel: 655–755 nm) under 405-nm excitation. Interestingly, numerous bright dots were observed in the cells for both channels (Figures 5a and 5b); this is largely different from what we observed for **PK**, which stained lipid compartments throughout the cells.[19] These dots were assigned as lipid droplets by conducting co-staining experiments using Lipi-Deep Red, a commercially available droplet-selective marker (Figure S5), and **PC**.[39] Notably, **PC** was found to selectively stain the lipid droplets, likely due to its hydrophobicity. Another interesting result was obtained when PC3 cells treated with triacsin C (5 μM), an inhibitor of lipid droplet formation,[40] were employed. Under this cell condition, the two channels provided different images (Figure 5d and 5e); in the red channel, **PC** was distributed into the intercellular membranes, especially those in the endoplasmic reticulum, whereas a small number of droplets were observed as small dots in the green channel. This observation could be explained by the fluorescence solvatochromic function of **PC**. Lipid droplets are known to be the least polar organelles in cells, whereas intercellular membranes are highly polar (often mimicked by DOPC LUVs[19]); as such, the fluorescence of **PC** in droplets and intercellular membranes could be emphasized using green and red channels, respectively. As a result, the droplets observed in the green channel were distinctly visualized as yellow-green color in the merged image (Figure 5f, white arrows in the merged image). These results indicate that under cell conditions where the formation of droplets is inhibited, **PC** can be distributed to both the remaining (or generated) lipid droplets and the intercellular membranes, which can be differentiated from one another. This might be a property unique to **PC** because Lipi-Deep Red simply loses its fluorescence outside the droplets.[39] Even when compared to **NR**, a traditional droplet marker, **PC** has advantages in terms of selectivity and photostability. Thus, **PC** could be a useful fluorescent tool for studying the dynamics of lipid droplets, including changes in their size, their morphology, and the number of them present under a given condition; this is notable considering that lipid droplets have recently attracted significant attention due to their role in cell starvation and stress.[13,41]

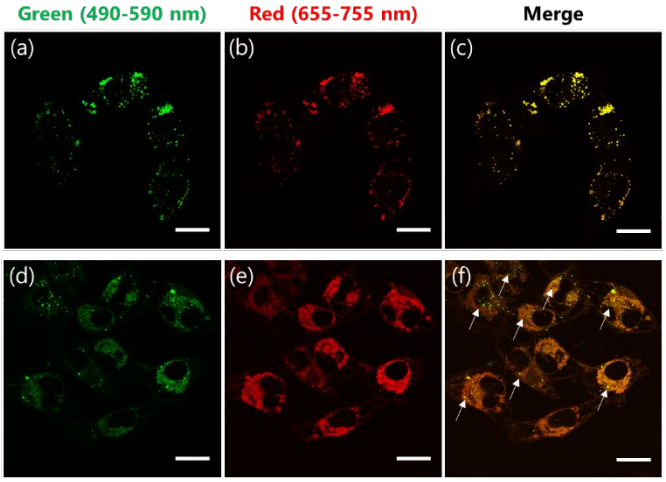

Figure 5. Confocal laser scanning fluorescence microscopy (CLSM) images of human prostate cancer cells (PC3 cells) (a–c) without and (d–f) with treatment using triacsin C. PC3 cells were stained with **PC**. White arrows in panel (f) point to portions of dots emphasized in the green channel. Probe concentration: 0.5 μM; excitation wavelength: 405 nm; scale bars: 20 μm.

Finally, the imaging of human skin tissue blocks fixed by paraformaldehyde was performed using 2PM (Figure 6). The tissues were embedded in paraffin, deparaffinized using xylene, and the resulting tissues were incubated with **PC** (10 μM) together with a transparency-enhancing agent (LUCID).[42] After washing to remove excess **PC** and LUCID, images were acquired under 960-nm excitation light, which is relatively tissue-penetrative among the wavelengths that a conventional titan-sapphire laser can operate (typically 700–1,040 nm) with sufficient output power.[43-45] The images were obtained using four channels: cyan (492 nm, for second harmonic generation), green (500–550 nm), orange (560–593 nm), and red (593–690 nm), and were then reconstructed to create 3D image stacks.

The near surfaces of tissue blocks ($z < 0.1$ mm, 2D images) were also visualized using a spectral imaging technique. As shown in Figure 6a, **PC** provided visuals of whole tissues via orange to red emissions. Interestingly, the fluorescence intensity of **PC** in the cell membranes is well pronounced; this is likely due to the anisotropic effect between the dye in the membrane and the excitation laser. As a result, the morphologies of individual cells in each tissue architecture, such as the stratum corneum, stratum lucidum, epidermis, and the basal cell layer, could be clearly observed. The use of **PK** gave rise to similar results through the green channel (Figure 6b), while **NR** provided a relatively blurry image (Figure S7), suggesting that the pyrene structure of **PC** might be advantageous for dye alignment into the lipid bilayer. Notably, **PC** provided much brighter images than **PK** under the same excitation power and enabled deeper tissue imaging in the z-axis direction. This is probably because **PC** exhibits a larger one-photon absorption coefficient (i.e., larger transition dipole moment) at 480 nm (i.e., half wavelength of 960 nm) than **PK** due to its red-shifted absorption (Figures 2a and 2b); therefore, **PC** has a larger two-photon absorption cross section than **PK**. In addition, the red-shifted emission of **PC** might also contribute to the increased imaging depth it provides. This feature of **PC**, efficiently driven by the 960-nm laser, offers various advantages for practical applications; for instance, to avoid tissue disruption, the use of 960-nm excitation is preferable to that of excitation at wavelengths < 900 nm. In addition, the use of 960-nm excitation is beneficial for co-staining experiments using a blue fluorescent dye, like DAPI (a nucleus-selective dye), based on three-photon excitation. In this context, the simultaneous deep skin tissue imaging of numerous large tissue blocks enabled by **PC** under 960-nm excitation is suitable for rapid and accurate biopsy applications.

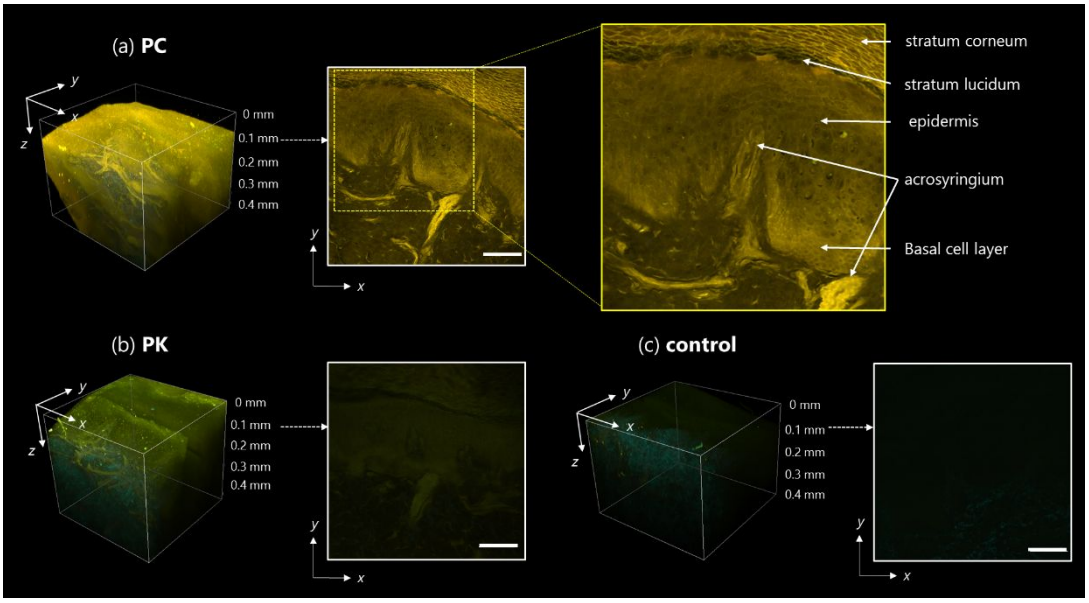

Figure 6. Two-photon fluorescence microscopy (2PM) images of normal human tissue blocks stained with (a) **PC**, (b) **PK**, or (c) a control (without probe). All tissues were treated with LUCID during the probe staining process to enhance their transparency. Probe concentration: 10 μM; excitation wavelength: 960 nm. 3D images were obtained from a cyan channel: 492 nm; a green channel: 500–550 nm; an orange channel: 560–593 nm, and a red channel: 593–690 nm. Near surfaces of tissue blocks (z < 0.1 mm, 2D images) were expressed using a spectral imaging technique; scale bars: 100 μm.

Conclusions

Herein, we developed a push–pull dye, **PC**, composed of pyrene, a piperidyl group, and a vinyl ketone. **PC** exhibits polarity-sensitive fluorescence from the green to far-red region due to its strong ICT characteristics, sufficiently high fluorescence quantum yield, and superior photostability to that of the commonly used green-to-red-emissive push–pull dye **NR**. Notably, **PC** stained model lipid membranes while showcasing fluorescence solvatochromism alongside a large change in fluorescence lifetime in response to the lipid compositions of the membranes. These fundamental properties of **PC** make it potentially applicable to various biological studies.

When **PC** was incubated with PC3, it rapidly and selectively stained the lipid droplets. Under the cell condition where the formation of lipid droplets were inhibited by triacsin C, **PC** could be distributed to both remaining droplets and intercellular membranes, while differentiating them through a merged image acquired by the green and red channels. This indicates that **PC** could be used as a fluorescent probe to monitor the dynamics of lipid droplets, such as changes in their size, their morphology, and the number of them present under a given condition. Furthermore, **PC** was found to efficiently stain fixed human tissue blocks in the presence of a transparency-enhancing agent. Using 2PM and tissue-penetrative 960-nm excitation light, **PC** provided bright images of the tissue blocks while revealing individual cells within each tissue architecture, enabling clearer and deeper tissue imaging than those provided by other solvatochromic dyes. This feature of **PC** would be significantly useful for rapid and accurate biopsy applications. Furthermore, **PC** is expected to be a suitable alternative to **PK**, a dye that has been previously used for human tissue imaging.

Thus, **PC** was revealed to have many attractive photophysical properties and several potential applications as a fluorescent probe for biological studies. Moreover, future studies modifying the **PC** structure could expand the applications of **PC** to include organelle targeting and advanced ratiometric and FLIM techniques. In fact, we are currently synthesizing new derivatives of **PC** for *in vivo* tissue imaging, which will be reported in the near future.

Experimental Section

Ethics

This study was conducted according to the principles of the Declaration of Helsinki. All subjects provided written informed consent and the work was approved by the Ethics Committee of Ehime University Graduate School of Medicine.

Reagents and materials

Unless otherwise noted, all commercial reagents and chemicals were used without further purification. The detailed procedure for the synthesis of **PC** is described in the Supporting Information. LUCID was prepared according to a previous method.[46]

Methods

Preparation of LUVs: LUVs were obtained by the extrusion method as previously described.[47] Briefly, a suspension of multilamellar vesicles was extruded using a NanoSizer Mini extruder (Funakoshi, Tokyo, Japan). The pore size of the filter was 100 nm (11 passages). This generated monodisperse LUVs with a mean diameter of 100 nm, as measured with a dynamic light scattering (DLS) system (nanoSAQLA, Otsuka Electronics, Osaka, Japan) based on the CONTIN method.

Preparation of PC3 cells: The human prostate cancer cell line PC3 was provided by Dr. Inoue (Kochi University, Kochi, Japan). The PC3 cells were maintained in Dulbecco's modified Eagle medium (DMEM) supplemented with 10% (v/v) fetal bovine serum (FBS, HyClone, Thermo Fisher Scientific, Waltham, USA) and a 1% (v/v) antibiotic antimycotic solution (09366-44, Nacalai Tesque, Kyoto, Japan). The cells were stored under 5% CO_2 gas at 37 °C.

Tissue sample preparation: Five skin samples from the fingertips of polydactyl patients were collected during operations. After removing the skin, tissue blocks (about 5 × 5 mm) were excised and then fixed in freshly prepared 4% (v/v) paraformaldehyde in phosphate buffer (pH 7.4) for 24–48 h at 4 °C; one block from each fingertip was embedded in paraffin. Sections with thicknesses of 500 μm were prepared for 2PM.

Characterization of materials: All ^{1}H NMR spectra were recorded using a 500 MHz JMN-LA500 instrument (JEOL Ltd., Tokyo, Japan) with tetramethylsilane as the internal standard. HRMS with electrospray ionization was performed using a Thermo Fisher Scientific LTQ Orbitrap XL mass spectrometer (Waltham, MA, USA).

Measurements of the photophysical properties: The absorption and fluorescence spectra were recorded with a V-670 UV–vis spectrophotometer (JASCO Corporation, Tokyo, Japan) and an FP6600 spectrofluorometer (JASCO Corporation), respectively. The absolute photoluminescence quantum yields were measured using a C9920-02 system (Hamamatsu Photonics K. K., Hamamatsu, Japan) equipped with an integral sphere. Fluorescence lifetimes were measured using a Quantaurus Tau fluorescence lifetime spectrometer (Hamamatsu Photonics K. K., Hamamatsu, Japan). All measurements were conducted at 298 K.

Cellular imaging using confocal laser scanning fluorescence microscopy: The cells were implanted from normal cell-culture dishes to a glass-bottom culture plate (EZVIEW, AGC Techno Glass, Tokyo, Japan) prior to confocal imaging. After adhesion, the cells were incubated with a 0.5 μM solution of **PC** containing Hank's balanced salt solution (HBSS) buffer for 30 min for confocal imaging. As for the experiment where the lipid droplet formation of the cells was inhibited (Figure 5b), the cells were first incubated with DMEM containing FBS and 5 μM of triacsin C for 18 h and then with **PC** containing HBSS buffer. An FV1000D downlight laser scanning confocal microscope (Olympus, Tokyo, Japan) was used for live-cell imaging. The excitation wavelength was set at 405 nm, and the emissions of the green and red channels were set at 490–590 nm and 655–755 nm, respectively. The laser illumination was set to 3.0% power. Images were acquired using a 100× oil immersion lens. Images were analyzed using the Olympus Fluoview ver. 4.2b software package.

Tissue imaging using two-photon fluorescence microscopy: Solutions of **PK** and **PC** (both 10 μM) were mixed in LUCID solution as a master mixed solution (Master Mix) for fluorescent staining, which was stored at room temperature before the staining procedure. Tissue sections with thicknesses of 500 μm were immersed in the Master Mix for over 76 h at room temperature. After that, tissue sections were imaged using an upright, confocal laser scanning microscope (A1R MP+, Nikon) with a Ti:Sa laser (MaiTai DS eHP, Spectra Physics, CA) fitted with a 25× water-immersion objective lens (Apo LWD 25×NA 1.10). The excitation laser frequency was 960 nm for all TPM imaging. To acquire second harmonic generation (SHG) signals, we divided the signals at 495 nm using a dichroic mirror. Fluorescent probe signals were detected at 500–550 nm, 563–593 nm, and 593–650 nm using x-y-z image acquisition (z-stack imaging) or spectroscopy during 2D image acquisition with a GaAsP-type photomultiplier module. The Z-stack sequences (step size, 5 μm), from the deepest level to the surface, corresponded to an area of 512 × 512 μm (1,024 × 1,024 pixels, 0.5 μm/pixel). The reconstructed 3D image stacks were subjected to median 3 × 3 filtering using NIS-Elements ver. 5.21 software (Nikon, Tokyo).

Author Contributions

Kazuki Inoue: Investigation, Writing – original draft, Writing – review & editing. **Ryosuke Kawakami:** Investigation. **Masamoto Murakami:** Investigation. **Teruko Tsuda:** Investigation. **Koji Sayama:** Investigation. **Takeshi Imamura:** Investigation. **Taku Nakayama:** Investigation. **Shinkuro Yamamoto:** Investigation. **Keiji Inoue:** Investigation. **Daisuke Kaneno:** Formal Analysis. **Shingo Hadano:** Investigation. **Shigeru Watanabe:** Investigation. **Yosuke Niko:** Conceptualization, Writing – original draft, Writing – review & editing.

Conflicts of interest

There are no conflicts to declare.

Acknowledgements

This research was supported by the Tobemaki Foundation, JSPS KAKENHI (grant number JP20K15246), and the Kochi University President's Discretionary Grant to Y.N. T.I. was supported by MEXT/JSPS KAKENHI (grant numbers JP16H06280, "Advanced Bioimaging Support", and JP15H05952 "Resonance Bio") and AMED (grant number JP20gm1210001). M.M, R.K, and Y.N. were supported by AMED under Grant Number JP20lm0203008. R.K., Y.N., and M.M. were supported by Adaptable and Seamless Technology Transfer Program through Target-driven R&D (A-STEP) from Japan Science and Technology Agency (JST) (grant number JPMJTM20RV). The authors are grateful to Ms. Megumi Kosaka and Ms. Tsugumi Shiokawa, Division of Instrumental Analysis, Okayama University, for the MS measurements. The computational work was performed at Research Center for Computational Science, Okazaki, Japan. Finally, we thank Ms. Hitomi Seki (Center for Photodynamic Medicine, Kochi Medical School, Kochi University) for her help in conducting fluorescence imaging using PC3 cells.

Notes and references

1 G. Weber and F. J. Farris, *Biochemistry*, 1979, **18**, 3075–3078.
2 P. Greenspan, E. P. Mayer and S. D. Fowler, *J. Cell Biol.*, 1985, **100**, 965–973.
3 S. Fery-Forgues, J. -P. Fayet and A. Lopez, *J. Photochem. Photobiol., A*, 1993, **70**, 229–243.
4 M. E. Vázquez, J. B. Blanco and B. Imperiali, *J. Am. Chem. Soc.*, 2005, **127**, 1300–1306.
5 B. E. Cohen, A. Pralle, X. J. Yao, G. Swaminath, C. S. Gandhi, Y. N. Jan, B. K. Kobilka, E. Y. Isacoff and L. Y. Jan, *Proc. Natl. Acad. Sci. U. S. A.*, 2005, **102**, 965–970.
6 P. D. Zoon and A. M. Brouwer, *ChemPhysChem*, 2005, **6**, 1574–1580.
7 Z. Lu, S. J. Lord, H. Wang, W. E. Moerner and R. J. Twieg, *J. Org. Chem.*, 2006, **71**, 9651–9657.
8 S. J. Lord, Z. Lu, H. Wang, K. A. Willets, P. J. Schuck, H. -l. D. Lee, S. Y. Nishimura, R. J. Twieg and W. E. Moerner, *J. Phys. Chem. A*, 2007, **111**, 8934–8941.
9 O. A. Kucherak, P. Didier, Y. Mèly and A. S. Klymchenko, *J. Phys. Chem. Lett.*, 2010, **1**, 616–620.
10 L. Giordano, V. V. Shvadchak, J. A. Fauerbach, E. A. Jares-Erijman and T. M. Jovin, *J. Phys. Chem. Lett.*, 2012, **3**, 1011–1016.
11 Y. Niko, S. Kawauchi and G. -i. Konishi, *Chem. - Eur. J.*, 2013, **19**, 9760–9765.
12 A. S. Klymchenko, *Acc. Chem. Res.*, 2017, **50**, 366–375.
13 K. Pal, T. Dutta and A. L. Koner, *ACS Omega*, 2021, **6**, 28–37.
14 A. S. Klymchenko and R. Kreder, *Chem. Biol.*, 2014, **21**, 97–113.
15 Y. Niko and A. S. Klymchenko, *J. Biochem.*, 2021, **170**, 163–174.
16 Y. Niko, Y. Cho, S. Kawauchi and G. -i. Konishi, *RSC Adv.*, 2014, **4**, 36480–36484.
17 Y. Niko, S. Sasaki, K. Narushima, D. K. Sharma, M. Vacha and G. -i. Konishi, *J. Org. Chem.*, 2015, **80**, 10794–10805.
18 Y. Niko, P. Didier, Y. Mely, G. -i. Konishi and A. S. Klymchenko, *Sci. Rep.*, 2016, **6**, 18870.

19 J. Valanciunaite, E. Kempf, H. Seki, D. I. Danylchuk, N. Peyriéras, Y. Niko and A. S. Klymchenko, *Anal. Chem.*, 2020, **92**, 6512–6520.
20 M. Murakami, R. Kawakami, Y. Niko, T. Tsuda, H. Mori, K. Yatsuzuka, T. Imamura and K. Sayama, *Acta Histochem. Cytochem.*, 2020, **53**, 131–138.
21 M. Murakami, R. Kawakami, Y. Niko, T. Tsuda, K. Yatsuzuka, H. Mori, T. Imamura and K. Sayama, *J. Dermatol. Sci.*, 2021, **102**, 130–132.
22 A. H. Ashoka, P. Ashokkumar, Y. P. Kovtun and A. S. Klymchenko, *J. Phys. Chem. Lett.*, 2019, **10**, 2414–2421.
23 T. Parasassi, E. K. Krasnowska, L. Bagatolli and E. Gratton, *J. Fluoresc.*, 1998, **8**, 365–373.
24 C. S. Lim, H. J. Kim, J. H. Lee, Y. S. Tian, C. H. Kim, H. M. Kim, T. Joo and B. R. Cho, *ChemBioChem*, 2011, **12**, 392–395.
25 C. S. Abeywickrama, K. J. Wijesinghe, R. V. Stahelin and Y. Pang, *Chem. Commun.*, 2017, **53**, 5886–5889.
26 C. S. Abeywickrama, K. J. Wijesinghe, C. B. Plescia, L. S. Fisher, T. GoodsonIII, R. V. Stahelin and Y. Pang, *Photochem. Photobiol. Sci.*, 2020, **19**, 1152-1159.
27 D. S. Surry and S. L. Buchwald, *Chem. Sci.*, 2011, **2**, 27–50.
28 M. Stephan, J. Panther, F. Wilbert, P. Ozog and T. J. J. Müller, *Eur. J. Org. Chem.*, 2020, **2020**, 2086–2092.
29 C. Reichardt, *Chem. Rev.*, 1994, **94**, 2319–2358.
30 M. Ravi, T. Soujanya, A. Samanta and T. P. Radhakrishnan, *J. Chem. Soc., Faraday Trans.*, 1995, **91**, 2739–2742.
31 E. Lippert, *Z. Elektrochem.*, 1975, **61**, 962–975.
32 N. G. Bakhshiev, *Opt. Spectrosk.* 1964, **16**, 821–832.
33 Z. R. Grabowski, K. Rotkiewicz and W. Rettig, *Chem. Rev.*, 2003, **103**, 3899–4031.
34 D. I. Danylchuk, P. -H. Jouard and A. S. Klymchenko, *J. Am. Chem. Soc.*, 2021, **143**, 912–924.
35 E. Sezgin, F. Schneider, V. Zilles, I. Urbančič, E. Garcia, D. Waithe, A. S. Klymchenko and C. Eggeling, *Biophys. J.*, 2017, **113**, 1321–1330.
36 D. I. Danylchuk, S. Moon, K. Xu and A. S. Klymchenko, *Angew. Chemie*, 2019, **131**, 15062–15066.
37 J. Rumin, H. Bonnefond, B. Saint-Jean, C. Rouxel, A. Sciandra, O. Bernard, J. -P. Cadoret and G. Bougaran, *Biotechnol. Biofuels*, 2015, **8**, 42.
38 Z. Darwich, A. S. Klymchenko, O. A. Kucherak, L. Richert and Y. Mély, *Biochim. Biophys. Acta - Biomembr.*, 2012, **1818**, 3048–3054.
39 Lipi-Deep Red: Technical manual is available online (http://www.dojindo.co.jp/manual/LD03e.pdf), January 24, 2022.
40 D. Matsuda, I. Namatame, T. Ohshiro, S. Ishibashi, S. Omura and H. Tomoda, *J. Antibiot.*, 2008, **61**, 318–321.
41 T. K. Fam, A. S. Klymchenko and M. Collot, *Materials*, 2018, **11**, 1768.
42 H. Mizutani, S. Ono, T. Ushiku, Y. Kudo, M. Ikemura, N. Kageyama, N. Yamamichi, M. Fujishiro, T. Someya, M. Fukayama, K. Koike and H. Onodera, *Pathol. Int.*, 2018, **68**, 102–108.
43 S. Chinnathambi and N. Shirahata, *Sci. Technol. Adv. Mater.*, 2019, **20**, 337–355.
44 M. Takezaki, R. Kawakami, S. Onishi, Y. Suzuki, J. Kawamata, T. Imamura, S. Hadano, S. Watanabe and Y. Niko, *Adv. Funct. Mater.*, 2021, **31**, 2010698.
45 Y. W. Jun, H. R. Kim, Y. J. Reo, M. Dai and K. H. Ahn, *Chem. Sci.*, 2017, **8**, 7696–7704.
46 H. Onodera, European Patent Office, EP2950077B1, 2014.
47 M. J. Hope, M. B. Bally, G. Webb and P. R. Cullis, *Biochim. Biophys. Acta - Biomembr.*, 1985, **812**, 55–65.